Assessment of the position accuracy of a single-frequency GPS receiver designed for electromagnetic induction surveys

Sebastian Rudolph[1,2]*, Ben Paul Marchant[3], Lutz Weihermüller[1] and Harry Vereecken[1]

[1] Forschungszentrum Jülich GmbH, Agrosphere Institute (IBG-3), Jülich, Germany (sebastian.rudolph@julumni.fz-juelich.de)

[2] Thünen Institute of Rural Studies, Braunschweig, Germany

[3] British Geological Survey, Environmental Science Centre, Keyworth, England

* Correspondence: sebastian.rudolph@julumni.fz-juelich.de; Tel.: +49-2461-61-8669

Acknowledgments: This study was supported by the Federal Ministry of Education and Research (Competence network for phenotyping science-CROP.SENSe.net). The contributions of B.P. Marchant are published with the permission of the Executive Director of the British Geological Survey (NERC).

Abstract: In precision agriculture (PA), compact and lightweight electromagnetic induction (EMI) sensors have extensively been used to investigate the spatial variability of soil, to evaluate crop performance, and to identify management zones by mapping soil apparent electrical conductivity (ECa), a surrogate for primary and functional soil properties. As reported in the literature, differential global positioning systems (DGPS) with sub-metre to centimetre accuracy have been almost exclusively used to geo-reference these measurements. However, with the ongoing improvements in Global Navigation Satellite System (GNSS) technology, a single state-of-the-art DGPS receiver is likely to be more expensive than the geophysical sensor itself. In addition, survey costs quickly multiply if advanced real time kinematic (RTK) correction or a base and rover configuration is used. However, the need for centimetre accuracy for surveys supporting PA is questionable as most PA applications are concerned with soil properties at scales above 1 m. The motivation for this study was to assess the position accuracy of a GNSS receiver especially designed for electromagnetic induction surveys supporting PA applications. Results show that a robust, low-cost and single-frequency receiver is sufficient to geo-reference ECa measurements at the within-field scale. However, ECa data from a field characterized by a high spatial variability of subsurface properties compared to repeated ECa survey maps and remotely sensed leaf area index (LAI) indicate that a lack of positioning accuracy can constrain the interpretability of such measurements. It is therefore demonstrated how relative and absolute positioning errors can be quantified and corrected. Finally, a summary of practical implications and considerations for the geo-referencing of ECa data using GNSS sensors are presented.

Keywords: Single-frequency GPS receiver; GNSS position accuracy, Electromagnetic induction (EMI) survey; ECa

Introduction

Precision agriculture (PA) is a crop management strategy, which aims to optimise field-level management with regard to crop farming, environmental protection, and economics. To understand the field-scale variability of crop status and environmental state properties new technologies such as airborne and satellite remote sensing, satellite based navigation systems, and geographical information systems (GIS) are being used (Bramley 2009). To minimise cost and effort of conventional point-by-point characterization of soil properties, mobile geophysical sensors, which can provide direct or indirect measurements of specific soil properties, have intensively been used in the last decade (Sudduth et al. 2001; Corwin 2008). Electromagnetic induction (EMI) measures soil apparent conductivity (ECa) by emitting an electromagnetic field while the response from the conductive subsurface is recorded. EMI instruments are the most commonly used geophysical sensors in PA and have been extensively used to investigate the spatial variability of soil, to estimate soil water content, clay content, soil depth, nutrient status, and also to evaluate crop performance, to identify crop management zones and to support agricultural experimentation (Eigenberg and Nienaber 2003; Jaynes et al. 1995; Kachanoski et al. 1988; Triantafilis and Lesch 2005; Frogbrook and Oliver 2007; Rudolph et al. 2016; Corwin 2008).

Commonly, EMI derived measurements are geo-referenced using a Global Navigation Satellite System (GNSS) such as the American Global Position System (GPS), the Chinese BeiDou Navigation Satellite System (BDS) or the Russian Global Navigation Satellite System (GLONASS). Using the GPS as an example, complex signals containing the precise time and orbital information are broadcasted by GNSS satellites in the form of the Coarse Acquisition Code (C/A code with 1.023 MHz), the Precise Code (P code with 10.23 MHz), and the navigation message (50 Hz) to the earth using different carrier frequencies in the L-band (1-2 GHz)(Kaplan and Hegarty 2006).

The GNSS receiver decodes respective information and calculates its geo-position based on the principles of triangulation. However, GNSS positioning accuracy is mainly constrained by satellite geometry, which describes the position of satellites relative to each other from the view of the receiver, atmospheric delay, a frequency dependent delay of the satellite signals passing through the troposphere and ionosphere, as well as multipath effects, caused by signal reflection from secondary sources (Leick et al. 2015).

In general, GNSS receivers can be distinguished based on the number of frequencies the sensor is capable of receiving (e.g. single-frequency (L1), multi-frequency systems (L1, L2, L5)), the concurrent reception of GNSS providers (e.g. single-constellation (GPS), multi-constellation (GPS/ GLONASS/BeiDou)), and whether code only or code and carrier-phase observations are used by the receiver (El-Rabbany 2006).

The advantages of the multi-frequency, multi-constellation systems are obvious. Atmospheric delay, multipath and receiver noise can be corrected by the concurrent reception of multiple frequencies, while balanced satellite geometry is more likely when information is received from as many satellites as possible. Furthermore, the navigation accuracy of the GNSS receiver considerably improves when pseudorange measurements, the distance between GNSS satellite and receiver, are obtained from the higher-resolution carrier-phase observations (wavelength 0.19 m) than from the code observations (wavelength 300 m) instead (Kaplan and Hegarty 2006). Moreover, real-time kinematic (RTK), which relies on differential carrier-phase observations, received by radio modems from either a nearby reference station or GSM (Global System for Mobile Communications), enables sub-centimeter levels of positioning.-These benefits have led the Australian Grains Research and Development Corporation to recommend differential GPS (DGPS) as the minimum level of accuracy for EMI surveys (O'Leary 2006).

However, modern geodetic-grade GNSS systems with centimetre accuracy are costly. Weltzien et al. (2003) reported an exponential relationship between GNSS accuracy and acquisition cost. At present, the costs for a fully operable multi-frequency, multi-constellation GNSS unit for commercial purpose starts above 15,000 € (personal communication Leica). In areas with insufficient GSM coverage an additional GNSS unit might have to be purchased to enable RTK correction. However, despite all possible upgrades a robust positioning performance cannot be guaranteed and the possible loss of the correction signal will inevitably cause artefacts in the positioning. Such erroneous survey observations have then either to be removed (Delefortrie et al. 2014) or corrected using post processing software (Kaplan and Hegarty 2006).

In contrast, a single-frequency GNSS receiver for less than 500 € might not be as accurate, but if the positioning accuracy of the receiver satisfies the demands of the proposed survey why should the surveyor not use a simpler GNSS unit? Beside acquisition costs, the requirement of a DGPS for ECa surveying is questionable as PA applications are generally concerned with soil properties measured on a scale above 1 m (McBratney and Pringle 1999) and most PA equipment only requires positioning with sub 3 m accuracy (McLoud et al. 2007). Furthermore, as most of the optical satellite imagery used in PA is sensed with a resolution of 5 x 5 m or above McBratney et al. (2003) proposed a pixel resolution of 5 x 5 m for proximal sensed high resolution soil survey maps.

Despites these arguments only a few published EMI studies have relied on a single-frequency GNSS receiver. For example, Francés and Lubczynski (2011) used a standard GPS receiver with a horizontal accuracy of ±2.5 m to reference EM-31 measurements, which they found to be satisfactory considering the scale of the spatial variation of surveyed clayey topsoil thickness. Similar GNSS systems were used by Vitharana et al. (2008), Mertens et al. (2008), López-Lozano et al. (2010), and Huang et al. (2014) to geo-reference ECa measurement taken in agricultural fields.

However, none of these studies highlighted accuracy-related issues for the interpretability of the resulting measurements. Furthermore, although the GNSS units utilised were optimised for good and stable navigation performance, the handheld receivers were designed for adventure outdoor activities and not to support geophysical surveys. Therefore, an affordable, robust and compact, easy to operate GNSS unit is needed for ECa survey supporting PA applications.

The objectives of this study were: i) to design an inexpensive L1 GNSS receiver for EMI surveys, ii) to quantify its position accuracy relative to an RTK-DGPS using static and dynamic measurements, iii) to quantify and correct positioning errors using repeated ECa measurements and secondary data.

Materials and Methods

The L1 GNSS system

The GNSS unit described here (expressed as EMI-GPS hereafter, see Figure 1) was designed to meet the needs of electromagnetic prospection surveys. Hardware components costing around 400 € were integrated into a compact (200x10x10 mm), robust, and waterproofed plastic housing. The core of the EMI-GPS is an Ublox LEA-6T (Thalwil, Switzerland) GPS. The single-frequency (L1 C/A code) GPS receiver operates with a maximal navigation update rate of 2 Hz and has a horizontal accuracy of 2.0 m with activated satellite-based augmentation system (SBAS) which accounts for satellite orbit and clock errors as well as atmospheric delay (Ublox 2010; Kaplan and Hegarty 2006). A compact Novatel ANT-537 L1 GPS patch antenna mounted on top of the plastic housing is used to receive GPS information. Position information in the form of the NMEA

(National Marine Electronics Association)(National Marine Electronics Association 2012) and the Ublox RAW format can either be recorded on an internal 2 GB SD-card or transmitted via an RS232 port to the geophysical sensor. The same port can be used to configure the module by Ublox u-center a freely available GNSS evaluation software(Ublox 2016), which allows the user to change between GNSS settings for different EMI sensors. The electronics of the EMI-GPS is powered by four easily replaceable AA Mignon Ni-MH rechargeable batteries, which last in operation for more than 12 h. Beside the low-cost and low-power consumption of the Ublox LEA-6T GPS module, the form factor ensures an easy upgrade to future Ublox LEA modules. Furthermore, the recorded RAW messages can be used by RTKLIB, a widely used, powerful, and highly portable open source software for real-time and post processing of GNSS data (Takasu and Yasuda 2009).

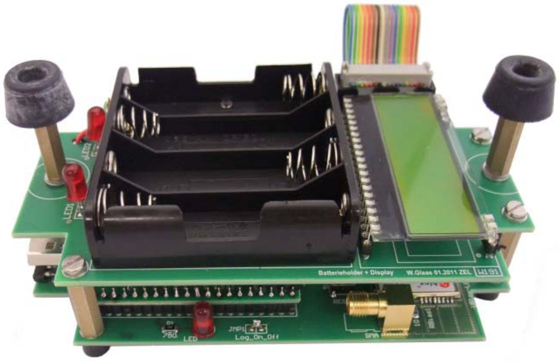

Figure 1. Electronic and hardware components of the EMI-GPS system depicted without the waterproofed plastic housing and GNSS antenna.

Assessment of the relative accuracy of the EMI-GPS determined by stationary recording

The most important parameter for validating GNSS receivers is the accuracy of positioning. This parameter is commonly assessed by the manufacturer based on static experiments in which the sensor is held fixed at a known location for a long time period (Taylor et al. 2004). However, since GNSS accuracy is subject to much marketing terminology, the accuracy should always be quantified under real operating conditions.

Therefore, a static performance test over 6 h was carried out at the TERENO test site Rollesbroich (Bogena et al. 2016). The site (50°37′33″N 6°18′19″E) is located 50 km west of Bonn (Germany) and is ideal for evaluating the GNSS receiver due to the absence of trees, buildings, and other tall objects. However, due to the remoteness of the area, the establishment of a stable RTK connection for correcting DGPS observations is challenging and for most of the time not possible. During the experiment, the EMI-GPS was placed on the ground and NMEA-GGA messages were recorded at 2 Hz to the internal SD-card.

The 2D accuracy of the receiver was quantified by calculating the Circular Error Probability (CEP), the Distance Root Mean Square parameter (DRMS), and two times this value, which is referred to as 2DRMS by Kaplan and Hegarty (2006). Each accuracy measure defines a radius from the true location describing a confidence region in which observations can be expected with a specific probability. The CEP is derived directly from the position error distribution and refers to the radius of a circle in which 50 % of the GNSS observations are measured. The CEP is calculated as:

$$CEP = 0.62 \ \ \delta_y + 0.56 \ \ \delta_x, \quad (1)$$

where δ_x and δ_y are the standard deviations of the longitudinal and latitudinal coordinates, respectively (NovAtel Inc. 2003). The DRMS defines a region in which 63-68 % of the observations are made and is calculated as:

$$DRMS = \sqrt{\delta_x{}^2 + \delta_y{}^2}. \quad (2)$$

The 2DRMS instead defines the area containing 95-98 % of the observations and is calculated as:

$$2DRMS = 2\sqrt{\delta_x{}^2 + \delta_y{}^2}. \quad (3)$$

As the true location of the EMI-GPS could not be determined by a DGPS the median of all observations was used as a reference point. For the analysis, coordinates had to be transformed from the global WGS84 into the metric UTM32 system and were then standardised on the reference coordinates. The dispersion of the horizontal error, calculated as the shortest distance between observations and the reference was then compared against the theoretical horizontal error distribution. The theoretical horizontal error function was derived from a Weibull distribution with scale parameter α=1 and shape parameter β=2 which is commonly used to model radial navigation errors (Kobayashi et al. 1992).

To further quantify the EMI-GPS measurements the position fix status, the number of satellites, as well as the Horizontal Dilution of Precision (HDOP) as provided by the NMEA-GGA messages, were analysed.

Assessment of the absolute accuracy of the EMI-GPS determined in a kinematic experiment

In addition to the stationary positioning, Taylor et al. (2004) noted that the reported accuracy of a GNSS receiver can vary significantly in dynamic mode. The position accuracy of two EMI-GPS receivers (expressed as Rover01 and Rover02 hereafter) was therefore compared against a NovaTel ProPak-V3 L1/L2 DGPS (NovAtel Inc., Calgary, Canada) with GSM-RTK correction in a kinematic experiment. Respective GNSS antennas were mounted at the same height and separated by 0.2 m with the DGPS antenna at central position on a test cart (see Fig. 3a), which was pulled at walking speed along the side markings of a road. Neither buildings nor other nearby obstacles affected the measurements. All GNSS observations were recorded as NMEA-GGA message with 1 Hz to the internal memory.

The robustness of the Rover observations were assessed by the following procedure. First, the closest DGPS location was determined for each Rover observation considering the recorded GPS time. Then, the direction of travel was reconstructed by fitting a smooth line through the six closest DGPS observations. Subsequently, the selected Rover observations were rotated around the DGPS reference location so that the direction of travel was pointing against north.

Under the assumption that the EMI-GPS would have recorded with almost perfect accuracy one should assume that the rotated Rover observations would cluster around a distinct position separated by 0.2 m from the origin, representing the DGPS reference location. Furthermore, the error distribution in longitudinal and latitudinal direction would be symmetric with its highest frequency at the centre. In contrast, a clustering further away from the reference as well as a distinct deviation from a circular pattern will indicate possible position errors, which can be described by descriptive statistics or the above-mentioned accuracy measures.

Quantification of the relative and absolute position accuracy of the EMI-GPS using ECa survey data and secondary data

In non-saline soils the spatial variation of ECa is primarily a function of soil texture, moisture content, and cation exchange capacity. Sudduth et al. (2001) showed that ECa patterns are spatially and temporally stable if the contribution of soil texture, especially clay content, dominates all other factors. Furthermore, a strong collinearity between shallow and deep ECa measurements can be expected. Recently, Rudolph et al. (2015) demonstrated that time variable crop-status patterns observed by multispectral satellite imagery can be linked to temporally stable ECa patterns. Hence, the relative positioning error of the EMI-GPS can be determined using repeatedly measured ECa data, while the absolute error can be assessedby using remotely sensed crop status measurements as reference. To quantify the relative and absolute positioning error ECa data of the TERENO site Selhausen - field F01 – from 2012 as well as an unpublished ECa dataset of the same field obtained in 2015 are considered. For both surveys, ECa data were obtained by the CMD miniExplorer (GFinstruments, Brno, Czech Republic) and measurements were geo-referenced by the above mentioned EMI-GPS. The EMI sensor consists of three receiver coils separated by $d_1 = 0.32$, $d_2 = 0.71$, and $d_3 = 1.18$ m from the transmitter coil. The resulting theoretical exploration depth for the vertical coplanar (VCP) mode ranges from 0 - 0.25 m (VCP1), 0 - 0.5 m (VCP2) and 0 - 0.9 m (VCP3) and for the horizontal coplanar (HCP) mode from 0 - 0.5 m (HCP1), 0 - 1.1 m (HCP2) and 0 - 1.9 m (HCP3), respectively. Due to the measurement principles of the EMI sensor, VCP and HCP data had to be obtained separately. For the published ECa survey VCP and HCP measurements were taken on two consecutive days, while for the later survey a second CMD miniExplorer was used to measure VCP and HCP simultaneously. In the so-called tandem-approach, both EMI sensors were pulled behind each other and geo-referenced separately. At any time the EMI-GPS was mounted in the center and 1.5 m above the EMI sensor while GNSS observations were transmitted to the ECa logger by 0.5 Hz. A detailed measurement setup is given by Rudolph et al. (2015).

Maps of the log-transformed and variance normalised ECa data were produced using geostatistical methods (Webster and Oliver 2007). A spatial autocorrelation amongst the data was represented by a Matérn variogram function (Minasny and McBratney 2005; Matérn 1986):

$$\gamma(h) = c_0 + c_1\left(1 - \frac{1}{2^{\nu-1}\Gamma(\nu)}\left(\frac{h}{a}\right)^{\nu} K_{\nu}\left(\frac{h}{a}\right)\right) \quad \text{for} \quad h > 0 \quad \text{and} \quad \gamma(0) = 0, \tag{4}$$

where h is the lag distance separating two observations, c_0 is the nugget variance describing the positive intercept on the ordinate for zero lag distance, and c_0+c_1 describe the sill variance of the variogram which equals the variance of the underlying population. Γ is the gamma function, K_ν denotes the modified Bessel function of the second kind, while $\nu > 0$ and $a > 0$ are smoothness and scale parameters, respectively. These parameters were estimated by the method of moments and then used to interpolate the ECa measurements to a raster with 0.25 m resolution using ordinary kriging (Webster and Oliver 2007).

For both ECa surveys, the relative position accuracy was assessed as follows. Within a search radius of 10 m, the interpolated VCP measurements were shifted stepwise in increments of 0.25 m relative to the HCP data. For each step, the Pearson correlation coefficient (r) was calculated between the position-corrected VCP and the measured HCP raster combinations (e.g. VCP1-HCP1, VCP1-HCP2, VCP1-HCP3). Respectively, the sum of all correlation coefficients was computed to quantify the positioning error. Assuming a strong collinearity between shallow VCP and deep HCP data, the relative position error would be indicated by the largest sum of all correlation coefficients. Once the error is obtained, the position of the VCP measurements can be corrected by applying the determined displacement vector.

In contrast, the absolute position accuracy was quantified similarly, but the interpolated VCP and HCP measurements were shifted and correlated against geo-referenced leaf area index measurements (LAI). Respective crop canopy measurements were taken in 2011 and are described by Rudolph et al. (2015). One should note, that larger observed LAI values indicated better crop performance under dry conditions due to a higher water holding capacity of the soil. As the water holding capacity is a function of clay content, similar patterns were described by the ECa survey. Zones of better crop performance were delineated manually in the western part of the field by a DGPS in 2013 as another severe drought period affected sugar beet. To evaluate the correction of the absolute error these delineated zones were visually compared with the measured and position corrected ECa data using a GIS. Furthermore, position-corrected ECa data were regressed with soil texture information as described by Rudolph et al. (2015) and the coefficients of determination (R^2) obtained were compared against the values derived from the measured ECa data.

Results and discussion

Relative accuracy of the EMI-GPS determined by the static performance test

Satellite visibility during the static performance test was good and the number of tracked satellites ranged from 8 to 12 with a median of 10. The high number of visible satellites resulted in an ideal satellite geometry as indicated by the HDOP, which varied between 0.75 and 1.2. A median HDOP of 0.8 indicated a very good satellite constellation (Kaplan and Hegarty 2006). The analysis of the position fix status information revealed that the first 51 observations were recorded without SBAS correction. The missing correction can be explained by the start mode of the receiver as well as the fact that the EMI-GPS is designed to record or transmit NMEA messages as soon as the receiver is switched on. In general, three start modes can be distinguished depending on the available GNSS information. If the receiver has no prior information about its current position, for example if the receiver was switched off for a longer time period and has been moved to another location, then information such as satellite constellation and UTC time have to be obtained before the new position can be determined. Hence, the so-called cold start is slower than the warm or hot start. As the EMI-GPS was set up to record its position at2 Hz, the first 26 s were affected by the missing correction. The same time period is given by the manufacturer of the LEA-6T GPS module for the cold start(Ublox 2010). Although, this time period is insignificant for a continuous EMI survey, warm up times should always be considered, especially for surveys at which the GNSS receiver is frequently switched on and off such as for a manual grid survey covering several hectares.

As summarised in Figure 2a, the recorded observations scatter within a radius of 2.3 m around the reference (median of all positions). The deviation from the reference was on average 0.76 m with a standard deviation of 0.41 m. CEP, DRMS and 2DRMS indicate that 50 % of the observations were made within 0.7 m, 68 % within 0.9 m and 98 % within 1.8 m. However, one should consider that in the reported experiment the system precision was accessed using the median of all measurements as a reference and that this approximation to the actual position contains a bias that will affect the results. Furthermore, as illustrated in Figure 2b the comparison between the measured and theoretical error distribution indicates a high frequency of small errors and a low frequency of larger errors. Since the comparison indicates that the horizontal measurement error was not entirely circular distributed nor Gaussian, the estimated CEP, DRMS and 2SDRMS values are likely to be underestimated due to the short observation time. In contrast, UBLOX quantifies the horizontal position accuracy of the LEA-6T module at2 m based on the CEP and a 24 h static performance test(Ublox 2010). Due to practical reasons, a longer observation time was not possible.

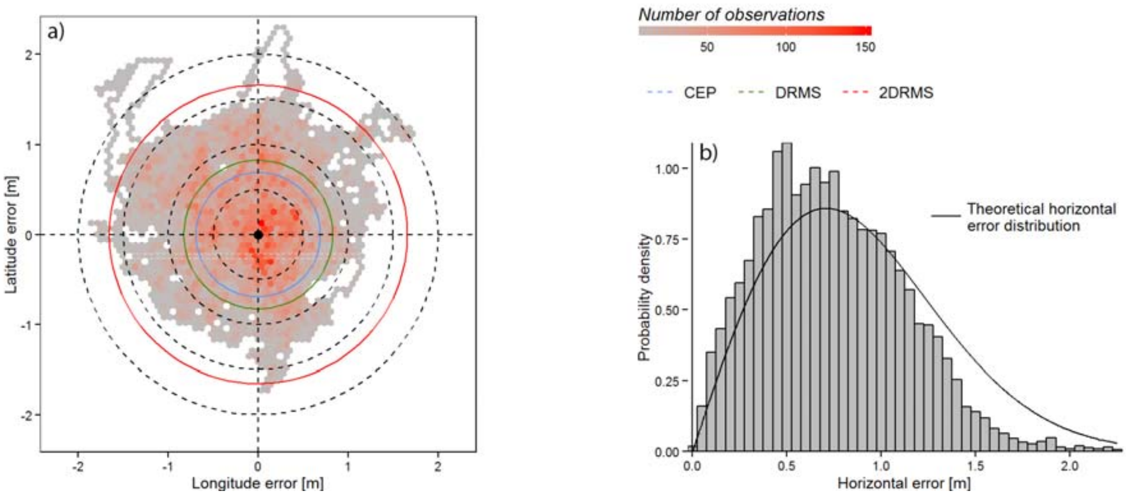

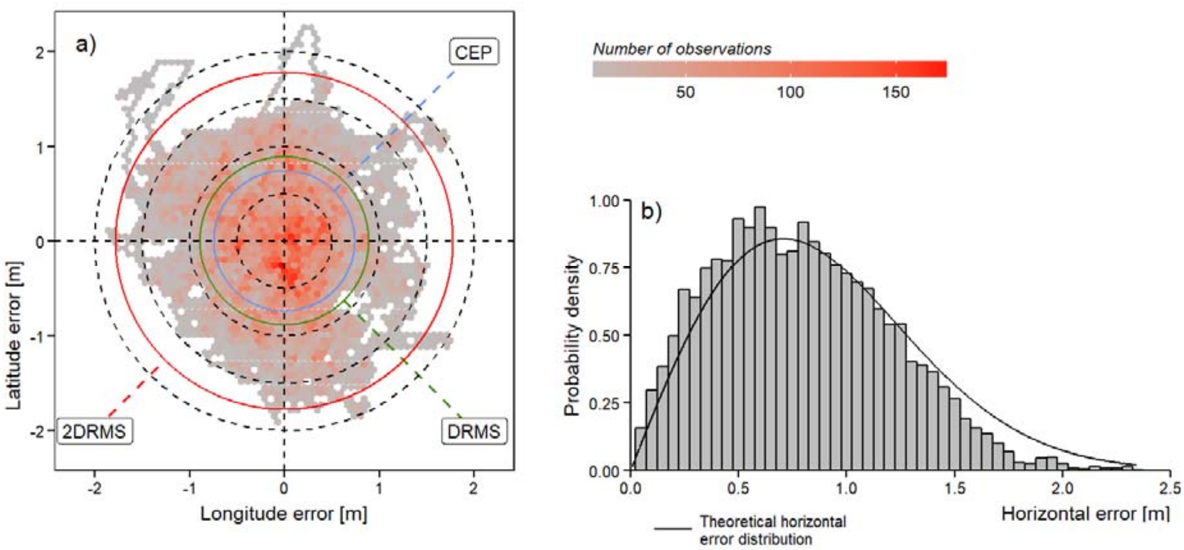

Figure 2. EMI-GPS observations of a 6 h static performance test. The scattering of all observations around its median quantified on the number of observations per area is illustrated in a) together with the Circular Error Probability (CEP), the Distance Root Mean square parameter (DRMS), and its double value the 2DRMS, which quantify the 2D accuracy of the EMI-GPS receiver during this experiment. In b) the dispersion of the observed horizontal error is compared against the theoretical horizontal error distribution derived from a Weibull distribution with scale parameter α=1 and shape parameter β=2.

Positioning accuracy of the EMI-GPS when operated in dynamic mode

During the kinematic experiment, satellite geometry was good as indicated by HDOP values which ranged for both Rover and the DGPS between 0.9 and 1.4. Larger differences were observed in the number of satellites used for position calculation. While the DGPS acquired on average seven satellites three more were used by the Rovers. These differences can possibly be explained by the antennas used as well as differences in the acquisition settings. For example, the elevation cut-off angle is a predefined parameter, which ensures that only satellites with a certain angle above the horizon are used by the receiver for position calculation. Although, a low cut-off angle generally results in a larger number of satellites it also increases the possibility of tropospheric or ionospheric delay, multipath errors, or blockage of the line-of-sight. In contrast, a high cut-off angle might exclude potential satellites and negatively affect the satellite constellation in view of the GNSS receiver. For the reported EMI-GPS measurements the default cut-off angle of 5° was used, whereas the angle used by the DGPS was unknown.

The analysis of the DGPS logs revealed that RTK correction had unnoticeably been lost three times during the data gathering and it took up to 2.5 minutes to re-establish the respective corrections (see Figure 3b). The RTK loss is illustrated in Figure 4 by comparing DGPS and Rover02 logs recorded along a 165 m long transect. As part of the 2.3 km long experimental track, the section was traversed twice. While DGPS observations logged with 1 Hz were in accordance with the road markings during the first pass a sudden jump and a varying offset of up to 2 m towards east indicates the loss of the RTK correction on the return (see Figure 4c and d). As soon as RTK-connection was re-established, DGPS recordings align perfectly as visualised in Figure 3b. In contrast, observations of Rover02 logged at 2 Hz showed no erratic behaviour at all but follow the reference track with a varying offset. However, the quantified position offset was at no time larger than for those of the DGPS without RTK correction.

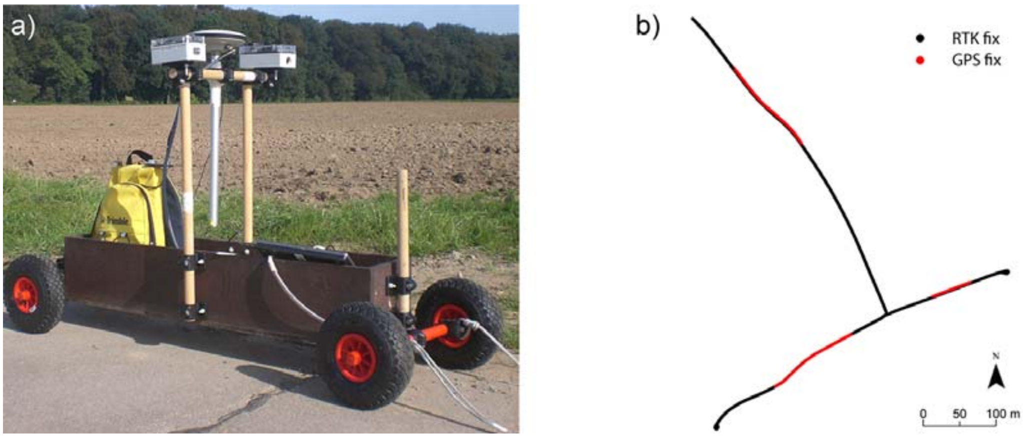

Figure 3. The experimental cart with the two EMI-GPS Rovers (Rover01 and Rover02) and the RTK corrected DGPS are depicted in a) while the layout of the test track colour-coded by the NMEA 0183 GPS quality indicator (National Marine Electronics Association 2012) is illustrated in b).

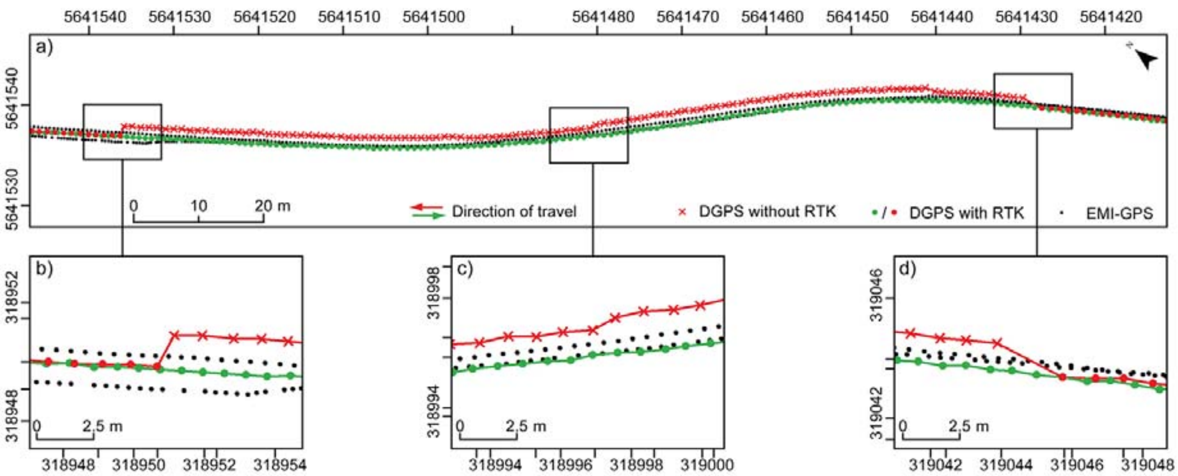

Figure 4. Comparison between the EMI-GPS and the DGPS observations along a 200 m long transect in the northern part of the experimental track. The loss of the RTK correction on the return (red colour) is illustrated in a). The sudden loss of respective correction is depicted in d) illustrated by the large offset in the DGPS observations. Subfigure c) and d) indicate that the EMI-GPS observations made in both directions are more similar than those made for the DGPS without RTK. The re-establishment of the RTK correction is illustrated in b).

The comparison of the EMI-GPS observation acquired in the kinematic and static experiment suggests that a kinematic filter algorithm is used by the LEA-6T GPS module as indicated by the good in-line alignment of respective observations. This assumption is strengthened by the fact that observations of both Rovers drifted away from the reference by up to 1.2 m as the cart stopped for 30 s (data not shown). However, the use of a filter, which smooths the signal to noise ratio as suggested in the literature, could not be verified by the information provided by the manufacturer (Ehrl et al. 2003).

The comparison between the DGPS reference and the rotated and normalised Rover observations are summarized in Table 1 and depicted in Figure 5a and b. Please note that DGPS observations recorded without RTK correction were removed previously. Although, Rover observations scattered within 2.5 m around the reference location, the scattering appeared to be unbalanced and more localised than compared to the static performance test. The high number of observations in the 3rd and 4th quadrant of the Cartesian coordinate system can partly be explained by the layout of the experiment as the majority of the observations were made along tracks in NW-SE (41 %) and SE-NW (23 %) directions. Furthermore, problems with the RTK correction occurred predominantly along the shorter NE-SW, and SW-NE segments of the track (see Figure 3b).

Table 1. Error quantification of the EMI-GPS observations referenced on a DGPS and obtained during the kinematic experiment.

EMI-GPS	Directional error [m]		Median distance [m]		GNSS quality measures [m]		
referenced on	Longitude	Latitude	Reference	DGPS path	CEP	DRMS	DRMS2
Rover01 on DGPS	-0.79 ± 0.53	-0.90 ± 0.58	1.22	0.72	0.66	0.79	1.58
Rover02 on DGPS	-0.63 ± 0.32	-1.01 ± 0.98	1.34	0.60	0.79	1.03	2.05
Rover02 on Rover01	-0.17 ± 0.80	-0.05 ± 0.88	0.82	-	0.99	1.18	2.37

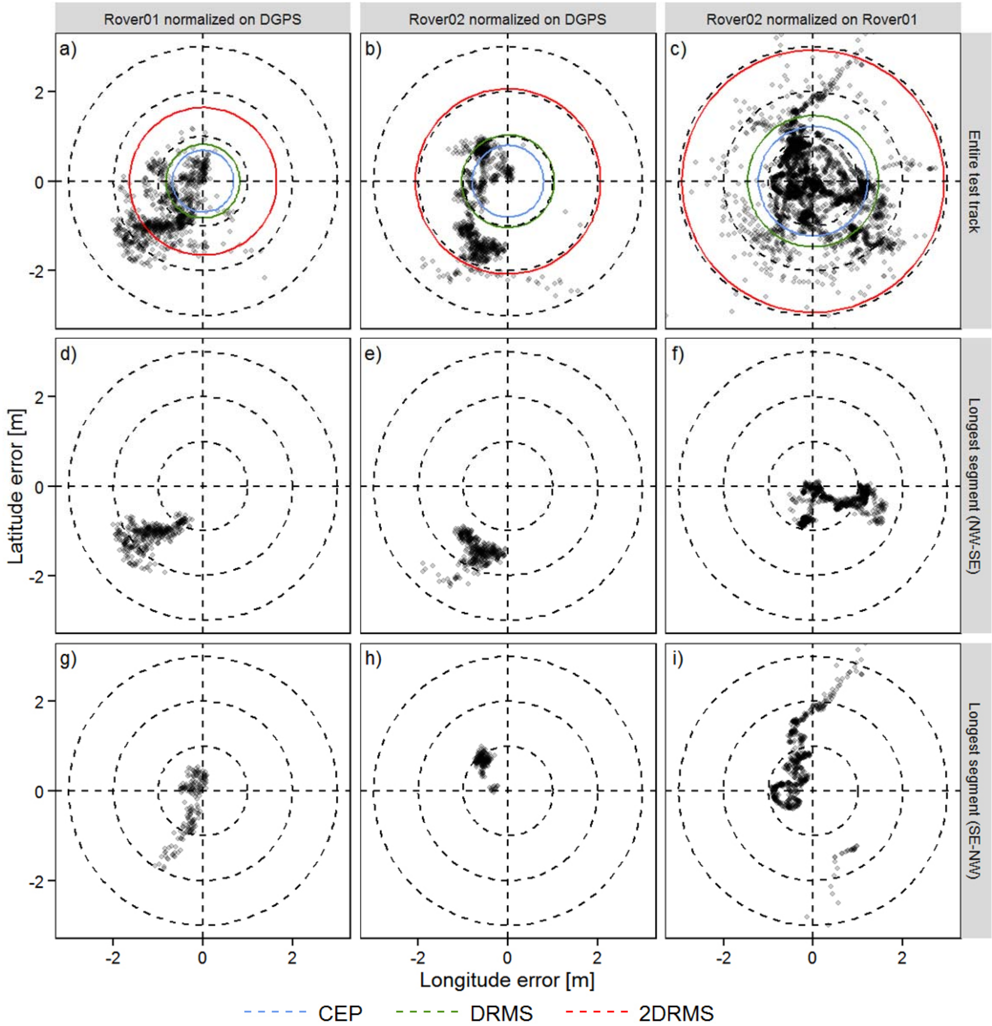
Rover01 normalized on DGPS
Rover02 normalized on DGPS
Rover02 normalized on Rover01
a)
b)
c)
d)
e)
f)
g)
h)
i)
Entire test track
Longest segment (NW-SE)
Longest segment (SE-NW)
Latitude error [m]
Longitude error [m]
2
0
-2
CEP
DRMS
2DRMS

326

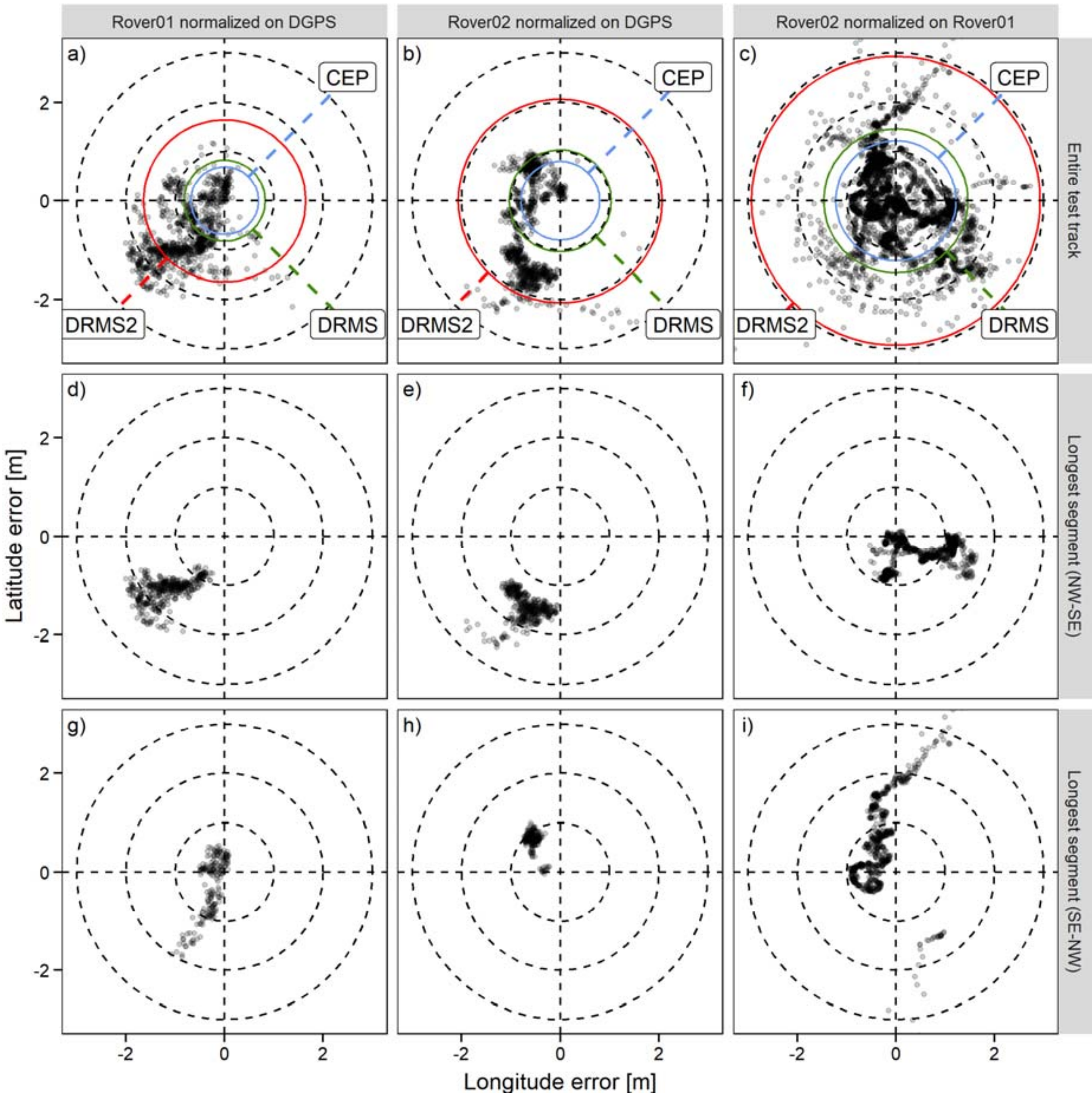

Figure 5. Comparison of the rotated and normalized EMI-GPS observations against the nearest RTK corrected DGPS location and against Rover01. The 2D accuracy of all EMI-GPS rover is quantified by the CEP, DRMS, and the 2DRMS in a – c). The dispersion of the standardized Rover observations taken in the NW-SE direction along the longest segment d-f) is compared against observations taken along the same segment on the return (g-i).

The median distance between the Rover observations and the DGPS reference location as well as towards the DGPS track was 1.22 m and 0.72 m for Rover01 and 1.34 m and 0.6 m for Rover02. The longitudinal error of Rover01 had a median of -0.79 m and a standard deviation of 0.53 m and was slightly larger than those of Rover02 (-0.63 ± 0.32 m). In contrast, a larger latitudinal error was obtained for Rover02 (-1.01 ± 0.98) than for Rover01 (-0.90 ± 0.58 m). The fact that observations of Rover01 were better circular distributed than those of Rover02 is reflected by the GNSS quality measures. For Rover01 a CEP of 0.66 m, a DRMS of 0.79 m, and a 2 DRMS of 1.58 m was obtained, while a CEP of 0.79 m, a DRMS of 1.03 m, and a 2DRMS of 2.05 m was calculated for Rover02. On the other hand, the normalisation of Rover02 on Rover01 indicated a more balanced distribution of the horizontal error between both Rovers. However, a CEP of 0.99 m, a DRMS of 1.18 m, and a 2DRMS of 2.37 m as well as a large standard deviation of the error ranging from 0.80 to 0.88 m suggests that both systems apparently obtained slightly different satellite information over time to calculate respective positions. Although, identical hardware components are used by the Rovers it can be assumed that the separation of Rover01 and Rover02 (see Figure 3a) by a multiple of the wavelength of the L1 frequency (~0.19 m) resulted in different multipath conditions and hence a different signal to noise ratio, which affected the system performance. Unfortunately, the recorded NMEA-GGA message does not provide further information and RAW messages were not recorded by the GNSS receivers.

The performance of both EMI-GPS receivers was further investigated along the longest segments of the test track. As illustrated in Figure 5d and e, the scattering of both Rovers indicates a similar position relative to the DGPS as the test chart was moved in the NW-SE direction. The apparent delay in the Rover positioning as suggested by the negative offset towards the DGPS can most likely be explained by the RTK-correction of the DGPS towards the south. This assumption is supported by Figure 5g and h which indicates a positive offset for most of the observations as the cart was pulled towards the opposite direction. Besides this, the comparison also indicates a more compact scattering of Rover02 compared to Rover01, especially on the return. This might explain the observed bi-modal distribution of the latitude error of Rover02. As summarised in Figure 5f and i deviations in the positioning between both systems occurred at any time with larger differences on the return.

Although, the kinematic experiment indicated a relatively small absolute position error one should note that the number of observations is relatively small (n = 1740). Furthermore, a more robust experimental design with a longer baseline and a balanced change of directions as well as a high number of repetitions under different satellite constellations is needed to quantify the position accuracy of the EMI-GPS further.

Quantification of the relative position accuracy of the EMI-GPS using EMI survey data

As illustrated in Figure 6, the estimated variograms of the ECa measurements from the 2012 and 2015 survey at the Selhausen site – field F01 -are remarkably similar. This is especially evident for the intermediate and deeper ECa data. Rudolph et al. (2015) showed that at this particular field, the clay content increased with depth. As the environmental conditions between the surveys were comparable, it is very likely that the spatial variability of the deeper measurements is controlled by the temporally stable clay content. The larger variation between the shallow VCP measurements can be related to the differences in the field management resulting in a different surface roughness and topsoil compaction (Brevik 2001).

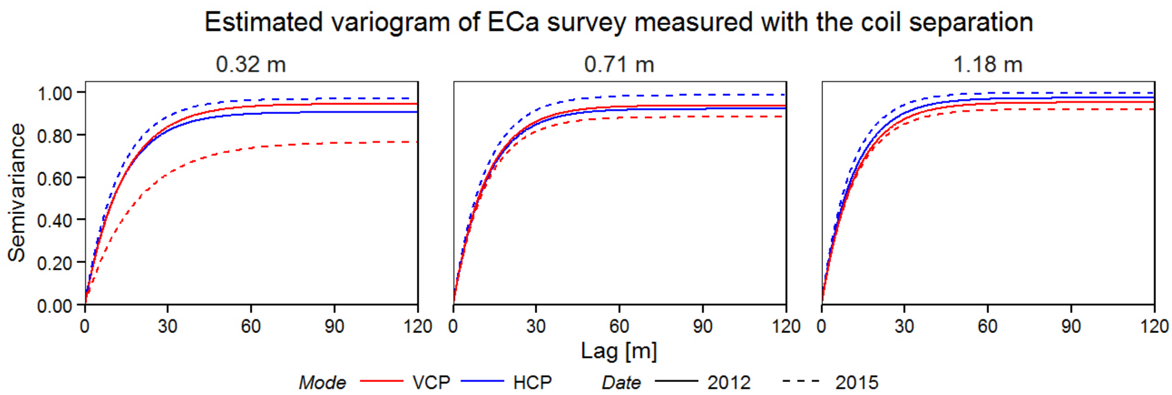

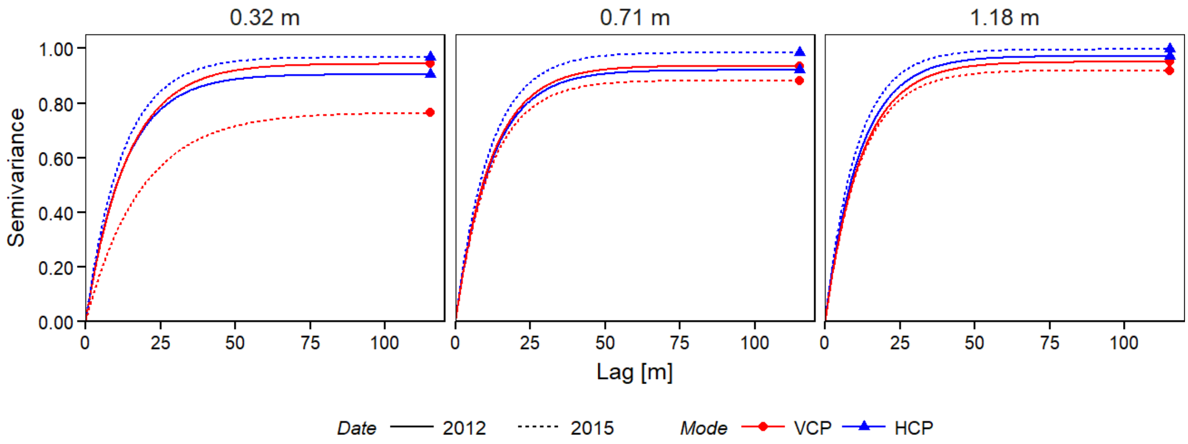

Figure 6. Comparison of the estimated spatial variability of the repeated 2012 and 2015 ECa survey at the TERENO test site Selhausen – field F01. Measurements were taken by the CMD miniExplorer in vertical coplanar (VCP) und horizontal coplanar (HCP) mode. The EMI sensor consists of three receiver coils separated by d_1 = 0.32, d_2 = 0.71, and d_3 = 1.18 m from the transmitter coil. The resulting theoretical exploration depth ranges from 0 - 0.25 m (VCP1), 0 - 0.5 m (VCP2), and 0 - 0.9 m (VCP3) and from 0 - 0.5 m (HCP1), 0 - 1.1 m (HCP2) and 0 - 1.9 m (HCP3), respectively.

The Pearson correlation coefficients calculated between the measured VCP and HCP raster indicate a good correlation for the 2012 survey ranging from 0.67 to 0.70 and a very good correlation for the 2015 survey ranging from 0.80 to 0.93 (see Table 2). The low correlation between the shallow ECa measurements are most likely an artefact of the smaller footprint and sensing depth of the sensor. Also the higher sensitivity of the EMI mode towards environmental conditions should be considered.

The assumption that the lower correlations of the 2012 survey were attributed to positioning errors was investigated by estimating the relative position error between respective ECa measurements. Using the sum of correlations estimated from a predefined set of offset combinations as a criterion, the estimated error distribution is visualised in Figure 7 and quantified in Table 2. The analysis revealed an elliptic shaped pattern with high correlations near the origin and lower correlations further away. One should note that the origin represents the initial correlation of the measured data. The location with the highest sum of correlations instead defines the offset which should be applied to the measured HCP data to achieve the highest correlation towards VCP. Respectively, the estimated position offset quantifies the magnitude of the relative error and describes the corresponding replacement vector. Figure 7a illustrates that for the 2012 survey, the highest correspondence between VCP and HCP measurements was found when HCP measurements were shifted by 5.5 m towards the east. As a consequence, the correlation significantly improved to 0.89 and 0.92 respectively. In contrast, Figure 7b illustrates the error distribution of the 2015 survey which suggests a relative error of only 1 m. As a consequence, only minor improvements were achieved, which do not show up in the summary statistics. As a consequence, the estimated error suggest that a tandem-approach, at which two EMI sensors were used simultaneously and geo-referenced individually, should be the preferred survey design as the effect of time-variable factors such as satellite constellation and atmospheric delay are minimal. However, multiple data sets from a variety of fields are needed to test this assumption further.

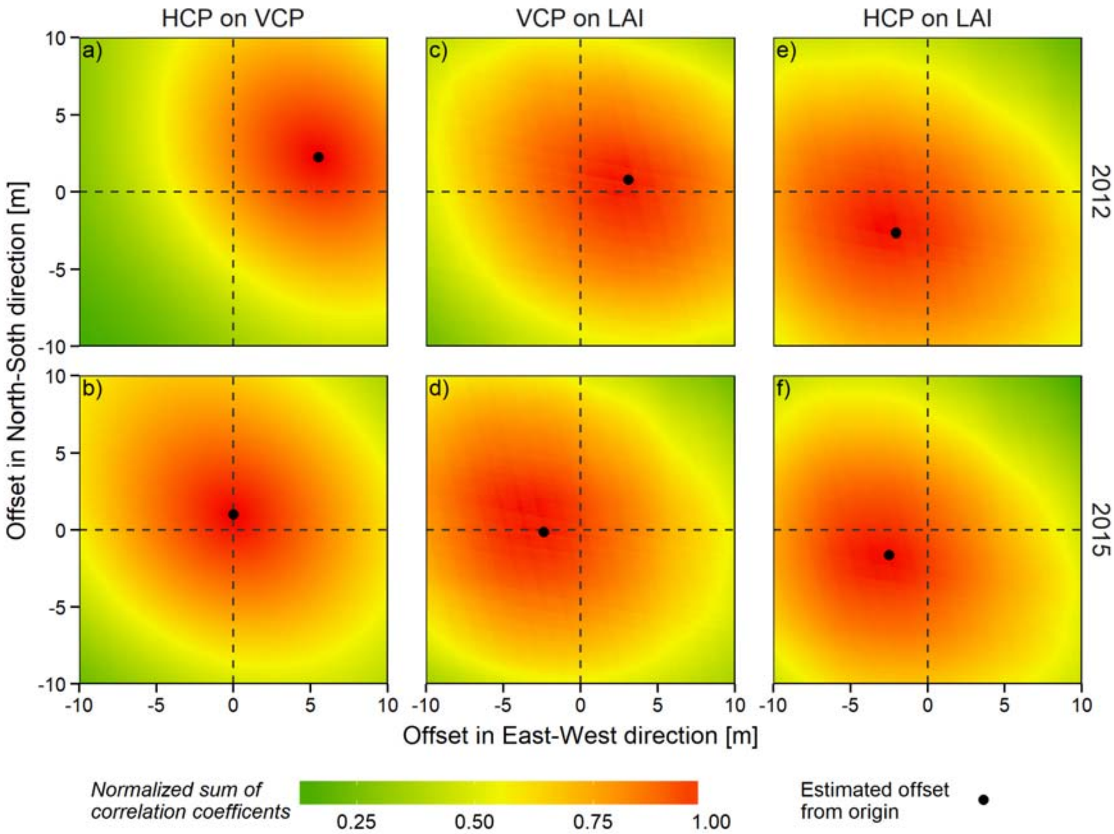

Figure 7. Comparison of the relative and absolute positioning error of the EMI-GPS receiver for two different survey designs. The relative positon error was assessed by stepwise correlating the shifted VCP against HCP measurements while the absolute positioning error was obtained by correlating remotely sensed leaf area index measurements (LAI) against the shifted VCP and HCP data. For both approaches the sum of the estimated Pearson correlation coefficient was used to quantify the error and replacement vector to correct the ECa data.

Quantification of the absolute positioning errors using remotely sensed LAI observations

The initial correlation between the geo-referenced LAI raster image and the shallow VCP measurements of the 2012 survey ranged between 0.47 and 0.62 (see Table 3). A slightly higher correlation was calculated for respective HCP measurements ranging from 0.60 to 0.68. The correlation coefficients between LAI and the 2015 ECa data were similar and ranged from 0.41 to 0.58. The determination and quantification of the absolute positioning error are visualised in Figure 7 c-f and summarised in Table 3. For the 2012 VCP measurements, the highest sum of correlation coefficients was determined by shifting the ECa raster by 3.2 m towards the east. In contrast, the highest correlation between LAI and HCP was located 3.35 m apart from the origin but in a westerly direction. The fact that both extrema were located in the opposite direction relative to the origin explains the previously determined large relative error. Although, a similar absolute position error was determined for the 2015 survey (2.4 and 3.0 m) the relative separation between both extrema was only 1 m. These findings are in good agreement with those made by the determination of the relative positioning error. The fact that the correlation between LAI and the position corrected ECa data improved only slightly, up to 0.73 for 2012 and 0.62 for 2015, can partly be attributed to the low resolution of the LAI raster of 5 x 5 m as well as the magnitude of the absolute positioning error. Furthermore, one should note that firstly, ECa and LAI observations were made in different years while secondly the observed spatial variability of LAI is not exclusively a function of soil texture. However, the assessment of the positioning error demonstrated that the position accuracy of an EMI survey can be validated and improved using affordable comprehensive secondary information. Certainly, the quantification of the positioning error of the EMI-GPS with a DGPS or self-tracking total station (TTS) would be more precise, but expensive to realise especially if more than one EMI device has to be geo-referenced.

Table 2. Comparison of the Pearson correlation coefficients obtained between measured and position corrected ECa data of the 2012 and 2015 EMI survey as well as quantification of the relative positioning errors and respective replacement vectors.

Survey date	**Correction method**	**Pearson correlation coefficient between respective EMI measurements**						**Estimated replacement vector of the absolute positioning error**			
		Original measured			Offset corrected						
		HCP1 vs VCP2	HCP2 vs VCP2	HCP3 vs VCP3	HCP1 vs VCP2	HCP2 vs VCP2	HCP3 vs VCP3	East-West offset [m]	North-South offset [m]	Angle [°]	Distance from optimum [m]
2012	VCP on HCP	0.67	0.69	0.70	0.89	0.90	0.92	5.50	2.25	22.25	5.94
2015	VCP on HCP	0.80	0.85	0.93	0.80	0.85	0.93	0.00	1.00	90.00	1.00

Table 3. Comparison of the Pearson correlation coefficient obtained between remotely sensed leaf area index (LAI) image and the measured and position corrected ECa raster of the 2012 and 2015 EMI survey as well as the quantification of the absolute positioning errors and respective replacement vectors.

Survey date	**Correction method**	**Pearson correlation coefficient between respective EMI measurements**						**Estimated replacement vector of the absolute positioning error**			
		Original measured			Offset corrected						
		HCP1 vs VCP2	HCP2 vs VCP2	HCP3 vs VCP3	HCP1 vs VCP2	HCP2 vs VCP2	HCP3 vs VCP3	East-West offset [m]	North-South offset [m]	Angle [°]	Distance from optimum [m]
24.07.2012	VCP on LAI	0.47	0.61	0.62	0.50	0.64	0.66	3.10	0.80	14.47	3.20
25.07.2012	HCP on LAI	0.60	0.66	0.68	0.65	0.70	0.73	-2.30	-2.35	-45.6	3.29
19.08.2015	VCP on LAI	0.41	0.56	0.58	0.44	0.59	0.61	-2.40	-0.15	-3.5763	2.40
19.08.2015	HCP on LAI	0.46	0.51	0.58	0.49	0.55	0.62	-2.50	-1.65	-33.424	3.00

Validation of the position corrected ECa data using independent secondary information

The comparison between the DGPS delineated zones of non-drought affected sugar beet as observed in 2013 and described by Rudolph et al. (2015) against the measured and position corrected ECa data normalised on its mean and standard deviation are depicted in Figure 8. The non-drought affected zones are well described by higher ECa values due to the high clay content in the subsoil. However, as indicated in Figure 8a-c slight deviations, especially for the first zone from the north as well as for the second zone from the south are obvious. While respective VCP measurements appear to be shifted towards the south-west the deeper HCP measurements tend to be positioned too far north. Although, these discrepancies can be of natural origin, ECa patterns almost align perfectly after the position was corrected using the geo-referenced LAI image raster (see Figure 8d-f).

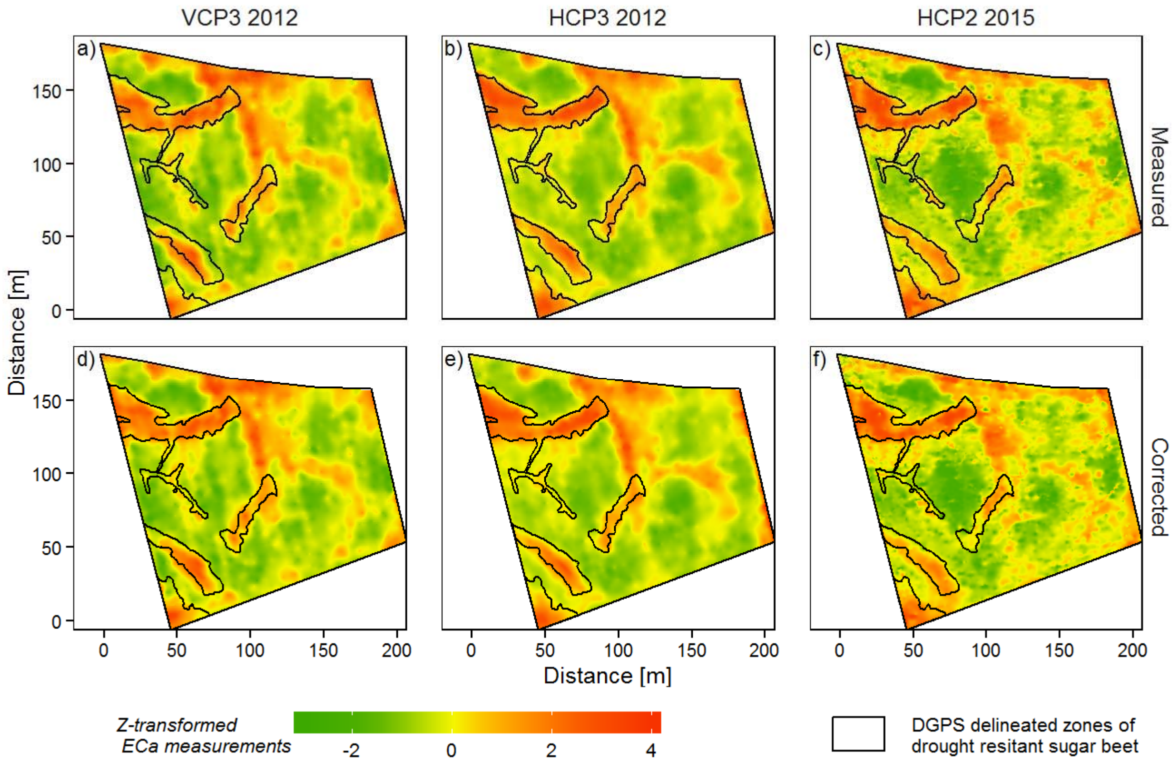

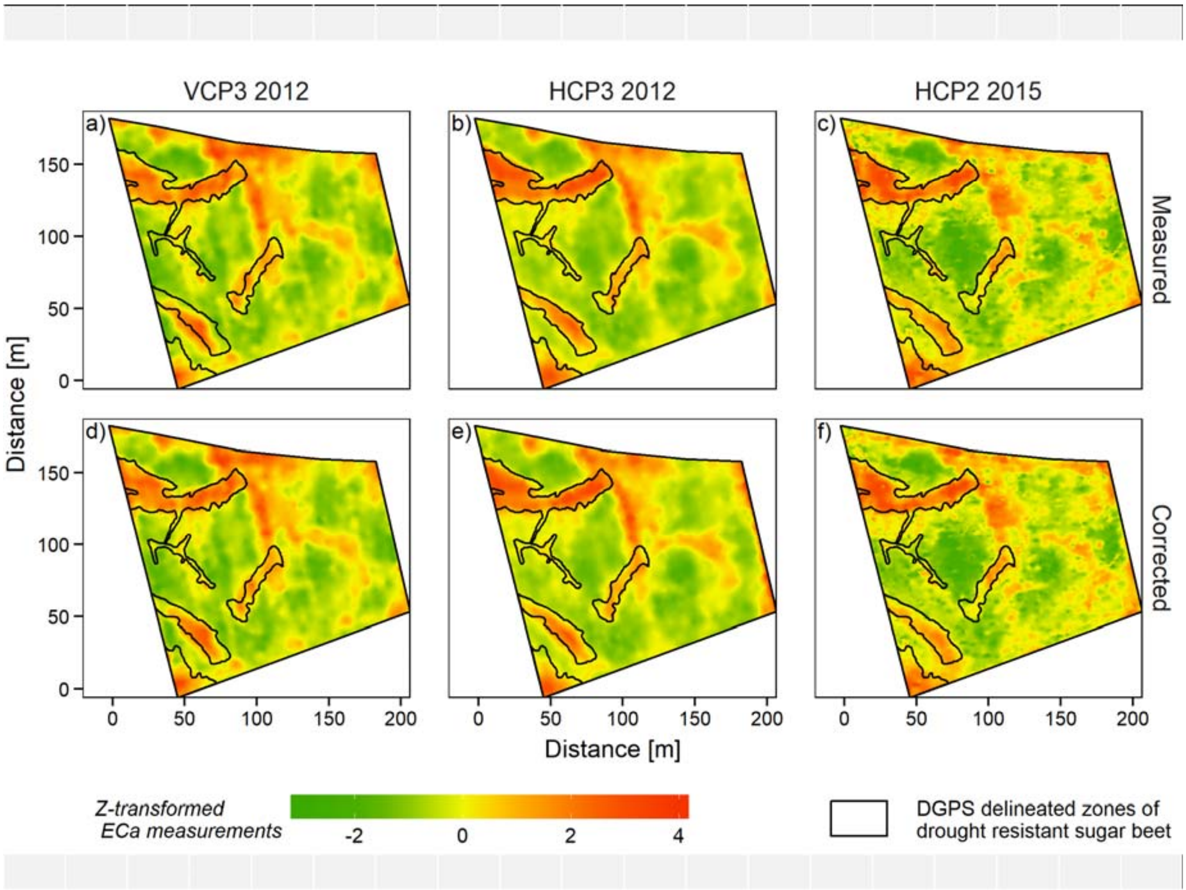

Figure 8. Comparison between the interpolated measured and position corrected ECa data against DGPS delineated zones of drought affected sugar beet.

To evaluate the correction of the absolute positioning error further, soil texture information obtained and described by Rudolph et al. (2015) were regressed against ECa. The coefficients of determination are compared in Table 4. Considerable improvements were found against topsoil texture for the 2015 ECa survey as well as the 2012 HCP measurements. In contrast, the position correction of the 2012 VCP measurements only slightly improved the prediction of subsoil clay content. Please note that the soil sampling campaign was directed by the LAI observations with the purpose ofdescribinge the transition in soil parent material within the narrow and undulating patterns. It is, therefore, understandable that the regression between ECa and soil texture improved as the position of ECa was corrected on LAI. In contrast, no or only minor improvements should have been expected if soil samples would have been taken within the homogeneous parts of the field.

Table 4. Comparison of the coefficients of determination (R^2) calculated between soil texture and the measured and position corrected ECa of the 2012 and 2015 EMI survey.

Survey date	EMI mode	Coefficient of determination (R^2)									
		Gravel		Sand topsoil		Silt topsoil		Clay topsoil		Clay subsoil	
		Before	After	Before	After	Before	After	Before	After	Before	After
2012	VCP1	0.43	0.40	0.14	0.10	0.32	0.20	0.23	0.18	0.23	0.24
	VCP2	0.53	0.50	0.26	0.20	0.40	0.28	0.31	0.28	0.53	0.54
	VCP3	0.53	0.51	0.32	0.25	0.42	0.31	0.34	0.29	0.59	0.65
	HCP1	0.32	0.50	0.07	0.16	0.14	0.30	0.21	0.32	0.33	0.34
	HCP2	0.34	0.54	0.13	0.25	0.13	0.33	0.25	0.35	0.62	0.57
	HCP3	0.39	0.54	0.16	0.27	0.16	0.33	0.27	0.33	0.68	0.65
2015	VCP1	0.19	0.11	0.01	0.00	0.04	0.01	0.08	0.07	0.09	0.02
	VCP2	0.32	0.40	0.05	0.10	0.07	0.14	0.17	0.33	0.19	0.25
	VCP3	0.40	0.52	0.12	0.20	0.13	0.24	0.23	0.34	0.46	0.40
	HCP1	0.37	0.45	0.11	0.21	0.09	0.19	0.30	0.33	0.40	0.37
	HCP2	0.36	0.53	0.13	0.23	0.08	0.23	0.29	0.36	0.45	0.47
	HCP3	0.40	0.54	0.17	0.31	0.13	0.29	0.29	0.36	0.61	0.56

Practical implications for the geo-referencing of ECa data using GNSS sensors

Based on the experiments conducted in this study using a DGPS and EMI-GPS the following practical implications should be considered for future EMI-surveys geo-referenced by any GNSS receiver.

First, the position accuracy of geodetic-grade DGPS receivers with RTK-correction is remarkably precise. However, most PA applications are carried out at remote locations where a reliable and stable GSM connection cannot be guaranteed. As an alternative, RTK corrections from a second nearby DGPS system can be used to precisely collect position information. However, the so-called base and rover configuration requires that the coordinates of the base station are known to obtain absolute measurements. Moreover, the loss of the RTK correction will introduce positioning errors which are difficult to correct using professional and costly post-processing software. Although, such erroneous observations can also be removed, one should consider that, depending on the survey speed, parts of the survey area will remain unsampled. Such gaps will irretrievably introduce uncertainty into the spatial estimation and interpolation of the property of interest.

Another factor which should be considered when using DGPS is a delay due to the latency of the DGPS. This is the time that a receiver needs to calculate and output the position, but also due to time lags in the data acquisition system (Sudduth et al. 2001). Both time lags will convert to a distance error depending on the speed of motion. Ehrl et al. (2003) showed that a DGPS has a considerably longer latency than a low-cost receiver due to the use of complex algorithms to determine its position. However, Lark et al. (1997) demonstrated that the delay can be estimated and corrected by minimizing the mean squared difference calculated between neighboring observations from adjacent passes and for a set of pre-defined offsets.

Second, SBAS corrected GNSS observations with an absolute positioning error of 2 m are sufficient for most PA applications. However, to guarantee optimal GNSS performance, the quality of the GNSS antenna as well as its positioning is crucial. Large performance differences mainly due to a less effective signal reception and multipath suppression have been reported between geodetic-grade and consumer-grade patch antennas (Takasu and Yasuda 2008; Pesyna et al. 2014; Odolinski and Teunissen 2016). To improve the signal quality one should first ensure that the antenna matches the technology of the GNSS receiver (Matias et al. 2015). Then, the antenna should be placed on a ground plane, such as a conductive plate, to reduce multipath and mounted at least 1.5 m above ground, apart from any electronic device to minimize radio-frequency interference. Furthermore, a cut-off angle of at least 15° is advisable but should be increased if required (Odolinski and Teunissen 2016). Moreover, the performance of the GNSS system should be at least once compared against a precise reference system such as a RTK-DGPS or TTS using stationary and dynamic measurements (Ehrl et al. 2003). If several GNSS positioning modules or antennas are available a sensitive test, in which the GNSS configuration to be tested is compared against a reference, should be considered to evaluate the best performing unit or configuration (Takasu and Yasuda 2008; Pesyna et al. 2014). Commonly used quality control parameters are the carrier-to-noise density or the signal-to-noise ratio (Kaplan and Hegarty 2006).

Third, when considering SBAS correction only, it is highly recommended to design the EMI survey carefully. As better accuracy is achieved along straight transects, measurements should be primarily carried out along evenly spaced transects, whereas the distance between them should be optimised regarding the expected accuracy of the GNSS receiver and the size of the survey area. Turning points instead should be located in the headland area or beyond field boundaries and survey interruption should be minimised if possible.

Fourth, if the purpose of the survey is to obtain ECa measurements from different depths by either using several EMI modes or several EMI device, one has to ensure that the measurements are taken over a relatively short time period to minimise factors such as satellite constellation and atmospheric delay. Note, that the satellite constellation for a given area can be predicted using freely available software such as the Trimble Planning Software (Trimble, Sunnyvale, USA). However, EMI devices which are capable of obtaining measurements from several depths without repeating the survey such as the EM-38DD or the Dual-EM´s are perfectly suited. In contrast, the combination of several sensors to the so-called tandem-approach has been presented as a promising alternative.

Fifth, to minimise interference between the GNSS and EMI unit (von Hebel et al. 2014) a number of published studies obtained position information from a DGPS placed with a spatial offset in front of the EMI sensor. Under the assumption that the sensor had followed in a straight line and at a constant distance the offset was corrected using sophisticated post-processing (see e.g. Sudduth et al. (2001); Gottfried et al. (2012); Delefortrie et al. (2014)). As a spatial offset adds uncertainty to the geostatistical estimation of the measured variable (Cressie and Kornak 2003), the use of a compact GNSS system centred above the EMI sensor within appropriate height is recommended.

Finally, even if position errors are apparent, respective measurements can be corrected using comprehensive secondary information, which can be related to the response variable. As an alternative, geo-referenced tracks collected along distinct features such as field boundaries or tram lines can be compared against remotely sensed images to quantify and correct respective measurements. However, one should note that the estimated position error will be variable between surveys if no RTK correction is used.

Conclusion

In this study, an affordable, single-frequency GPS system developed for EMI surveys supporting PA applications was introduced. Comparisons between the EMI-GPS and a RTK-DGPS with centimetre accuracy indicated that the averaged absolute position error never exceeded 1.5 m. While the DGPS occasionally suffered from weak RTK correction no erratic behaviour was evident for the EMI-GPS. ECa survey data indicates a good accuracy of the EMI-GPS along straight transects with a higher variation in the positioning at turning points or at fixed locations. Moreover, ECa data suggests that the absolute positioning error of the EMI-GPS remained constant over the period of a survey but varied between surveys. Furthermore, data indicates that the relative positioning error was larger when measurements were obtained on different dates. To minimise the effects of time variable factors such as satellite constellation and atmospheric delay the concurrent measurement of both shallow and deep EMI modes is proposed. Finally, geo-referenced ECa data suggest that for most PA applications the low-cost, single-frequency EMI-GPS is a promising alternative to the expensive geodetic-grade RTK-DGPS systems.

Conflicts of interest: The authors declare no conflict of interest.

References

Bogena, H., Borg, E., Brauer, A., Dietrich, P., Hajnsek, I., Heinrich, I., et al. (2016). TERENO: German network of terrestrial environmental observatories. *Journal of large-scale research facilities, 2*(A52).

Bramley, R. G. V. (2009). Lessons from nearly 20 years of Precision Agriculture research, development, and adoption as a guide to its appropriate application. *Crop & Pasture Science, 60*(3), 197-217.

Brevik, E. C. (2001). *Evaluation of selected factors that may influance the application of electromagnetic induction technology to soil science investiagtion in Iowa*. Iowa State University, Ames, Iowa.

Corwin, D. L. (2008). Past, present, and future trends of soil electrical conductivity measurements using geophysical methods. In B. Allred, J. J. Daniels, & M. R. Ehsani (Eds.), *Handbook of Agricultural Geophysics* (pp. 17-44): CRC Press.

Cressie, N., & Kornak, J. (2003). Spatial statistics in the presence of location error with an application to remote sensing of the environment. *Statistical Science, 18*(4), 436-456.

Delefortrie, S., De Smedt, P., Saey, T., Van De Vijver, E., & Van Meirvenne, M. (2014). An efficient calibration procedure for correction of drift in EMI survey data. *Journal of Applied Geophysics, 110*, 115-125.

Ehrl, M., Stempfhuber, W., Auernhammer, H., & Demmel, M. Quality assessment of agricultural positioning and communication systems. In J. V. Stafford, & A. Werner (Eds.), *Precision agriculture: Proceedings of the 4th European Conference on Precision Agriculture, Berlin, 15-19 June 2003 2003* (pp. 205-210): The Netherlands: Wageningen Academic Publishers

Eigenberg, R. A., & Nienaber, J. A. (2003). Electromagnetic induction methods applied to an abandoned manure handling site to determine nutrient buildup. *Journal of Environmental Quality, 32*, 1837-1843.

El-Rabbany, A. (2006). *Introduction to GPS: The Global Positioning System* (Vol. 2). Massachusetts, United States: Artech House.

Francés, A. P., & Lubczynski, M. W. (2011). Topsoil thickness prediction at the catchment scale by integration of invasive sampling, surface geophysics, remote sensing and statistical modeling. *Journal of Hydrology, 405*, 31-47.

Frogbrook, Z. L., & Oliver, M. A. (2007). Identifying management zones in agricultural fields using spatially constrained classification of soil and ancillary data. *Soil Use and Management, 23*, 40-51.

Gottfried, T., Auerswald, K., & Ostler, U. (2012). Kinematic correction for a spatial offset between sensor and position data in on-the-go sensor applications. *Computers and Electronics in Agriculture, 84*, 76-84.

Huang, J., Nhan, T., Wong, V. N. L., Johnston, S. G., Lark, R. M., & Triantafilis, J. (2014). Digital soil mapping of a coastal acid sulfate soil landscape. *Soil Research, 52*(4), 327-339.

Jaynes, D. B., Colvin, T. S., & Ambuel, J. Yield mapping by electromagnetic induction. In P. C. Robert, R. H. Rust, & W. E. Larson (Eds.), *Proceedings of the Second International Conference on*

Precision Agriculture. Madison, WI, USA, Minneapolis, 1995 (pp. 383-394). no: ASA-CSSA-SSA

Kachanoski, R. G., Gregorisch, E. G., & van Wesenbeeck, I. J. (1988). Estimating spatial variations of soil water content using noncontacting electromagnetic inductive methods. *Canadian Journal of Soil Science, 68*, 715-722.

Kaplan, E. D., & Hegarty, C. J. (2006). *Understanding GPS - Principles and Applications* (2ed.). Massachusetts, United States: Artech House.

Kobayashi, M., Ingels, F., & Bennett, G. (1992). *Determination of the probability density function of GPS (Global Positioning Systems) positioning error.* Paper presented at the Proceedings of the 48th annual meeting of the institute of navigation, Dayton,

Lark, R. M., Stafford, J. V., & Bolam, H. C. (1997). Limitations on the spatial resolution of yield mapping for combinable crops. *Journal of Agricultural Engineering Research, 66*(3), 183-193.

Leick, A., Rapoport, L., & Tatarnikov, D. (2015). *GPS satellite surveying* (Fourth edition. ed.). New Jersey, USA: Wiley.

López-Lozano, R., Casterad, M. A., & Herrero, J. (2010). Site-specific management units in a commercial maize plot delineated using very high resolution remote sensing and soil properties mapping. *Computers and Electronics in Agriculture, 73*, 219-229.

Matérn, B. (1986). *Spatial Variation* (Vol. 36, Lecture Notes in Statistics). New York, USA: Springer.

Matias, B., Oliveira, H., Almeida, J., Dias, A., Ferreira, H., Martins, A., et al. High-accuracy low-cost RTK-GPS for an unmannned surface vehicle. In *OCEANS 2015, Genova, Italy 18-21 May 2015 2015* (pp. 1-4): IEEE

McBratney, A. B., & Pringle, M. J. (1999). Estimating average and proportional variograms of soil properties and their potential use in Precision Agriculture. *Precision Agriculture, 1*(2), 125-152.

McBratney, A. B., Santos, M. L. M., & Minasny, B. (2003). On digital soil mapping. *Geoderma, 117*(1-2), 3-52.

McLoud, P. R., Gronwald, R., & Kuykendall, H. (2007). Precision agriculture: NRCS support for emerging technologies. Agronomy Technical Note No.1. Washington, USA.

Mertens, F. M., Pätzold, S., & Welp, G. (2008). Spatial heterogeneity of soil properties and its mapping with apparent electrical conductivity. *Journal of Plant Nutrition and Soil Science, 171*, 146-154.

Minasny, B., & McBratney, A. B. (2005). The Matern function as a general model for soil variograms. *Geoderma, 128*(3-4), 192-207.

National Marine Electronics Association (2012). NMEA 0183, The Standard for Interfacing Marine Electronics. New Bern, USA: www.nmea.org.

NovAtel Inc. (2003). GPS Position Accuracy Measures. APN-029 Rev 1. Calgary, Canada.

O'Leary, G. (2006). Standards for electromagnetic induction mapping in the grains industry. In J. Peters (Ed.), *GRDC Precision Agriculture Manual* Barton, Australia: Grains research and development corporation.

Odolinski, R., & Teunissen, P. J. G. (2016). Single-frequency, dual-GNSS versus dual-frequency, single-GNSS: a low-cost and high-grade receivers GPS-BDS RTK analysis. *Journal of Geodesy, 90*(11), 1255-1278.

Pesyna, K. M. J., Heath, R. W. J., & Humphreys, T. E. Centimeter positioning with a smartphone-quality GNSS Antenna. In *27th international technical meeting of the satellite division of the Institute of Navigation, Tampa, USA, 2014* (pp. 1568-1577): ION Publications

Rudolph, S., van der Kruk, J., von Hebel, C., Ali, M., Herbst, M., Montzka, C., et al. (2015). Linking satellite derived LAI patterns with subsoil heterogeneity using large-scale ground-based electromagnetic induction measurements. *Geoderma, 241-242*, 262-271.

Rudolph, S., Wongleecharoen, C., Lark, R. M., Marchant, B. P., Garré, S., Herbst, M., et al. (2016). Soil apparent conductivity measurements for planning and analysis of agricultural experiments: A case study from Western-Thailand. *Geoderma, 267*, 220-229.

Sudduth, K. A., Drummond, S. T., & Kitchen, N. R. (2001). Accuracy issues in electromagnetic induction sensing of soil electrical conductivity for precision agriculture. *Computers and Electronics in Agriculture, 31*(3), 239-264.

Takasu, T., & Yasuda, A. Evaluation of RTK-GPS performance with low-cost single-frequency GPS receivers. In *International symposium on GPS/GNSS 2008, Tokyo, Japan, 2008* (pp. 852–861)

Takasu, T., & Yasuda, A. Development of the low-cost RTK-GPS receiver with an open source program package RTKLIB. In *International Symposium on GPS/GNSS, Jeju, Korea, 2009* (pp. 4-6)

Taylor, R. K., Schrock, M. D., Bloomfield, J., Bora, G., Brockmeier, G., Burton, W., et al. (2004). Dynamic testing of GPS receivers. *Transactions of the ASAE, 47*(4), 1017-1025.

Triantafilis, J., & Lesch, S. M. (2005). Mapping clay content variation using electromagnetic induction techniques. *Computers and Electronics in Agriculture, 46*(1-3), 203-237.

Ublox (2010). LEA-6 u-blox 6 GPS modules data sheet. Thalwil, Swiss.

Ublox (2016). U-center: GNSS evaluation software for Windows. Thalwil, Swiss.

Vitharana, U. W. A., van Meirvenne, M., Simpson, D., Cockx, L., & de Baerdemaeker, J. (2008). Key soil and topographic properties to delineate potential management classes for precision agriculture in the European loess area. *Geoderma, 143*, 206-215.

von Hebel, C., Rudolph, S., Mester, A., Huisman, J. A., Kumbhar, P., Vereecken, H., et al. (2014). Three-dimensional imaging of subsurface structural patterns using quantitative large-scale multiconfiguration electromagnetic induction data. *Water Resources Research, 50*(3), 2732-2748, doi:10.1002/2013wr014864.

Webster, R., & Oliver, M. A. (2007). *Geostatistics for environmental scientists*. Chichester, UK: John Wiley & Sons Ltd.

Weltzien, C., Noack, P. O., & Persdson, K. GPS receiver accuracy test - dynamic and static for best comparison of results. In J. Stafford, & A. Werner (Eds.), *Proceedings of the 4th European Conference on Precision Agriculture, Berlin, 2003* (pp. 717-722): The Netherlands: Wageningen Academic Publishers